npj computational materials

www.nature.com/npjcompumats

ARTICLE OPEN

Hybrid magnetorheological elastomers enable versatile soft actuators

Miguel Angel Moreno-Mateos[1]✉, Mokarram Hossain[2], Paul Steinmann[3,4] and Daniel Garcia-Gonzalez[1]✉

Recent advances in magnetorheological elastomers (MREs) have posed the question on whether the combination of both soft- and hard-magnetic particles may open new routes to design versatile multifunctional actuators. Here, we conceptualise ultra-soft hybrid MREs (≈1–10 kPa stiffness) combining experimental and computational approaches. First, a comprehensive experimental characterisation is performed. The results unravel that the magneto-mechanical performance of hybrid MREs can be optimised by selecting an adequate mixing ratio between particles. Then, a multi-physics computational framework provides insights into the synergistic magneto-mechanical interactions at the microscale. Soft particles amplify the magnetisation and hard particles contribute to torsional actuation. Our numerical results suggest that the effective response of hybrid MREs emerges from these intricate interactions. Overall, we uncover exciting possibilities to push the frontiers of MRE solutions. These are demonstrated by simulating a bimorph beam that provides actuation flexibility either enhancing mechanical bending or material stiffening, depending on the magnetic stimulation.

npj Computational Materials (2022)8:162 ; https://doi.org/10.1038/s41524-022-00844-1

INTRODUCTION

Intelligent materials responding to external magnetic stimuli have revolutionised soft robotics, smart sensors and bioengineering fields. Such smart multi-functional materials provide groundbreaking solutions to remotely modulate material properties, such as stiffness changes or shape-morphing phenomena. Some relevant applications are due to the untethered navigation of soft robots within soft biological matter[1–5], or magneto-active substrates for non-invasive cell stimulation[1,6–9]. Other applications impacted by this disruptive technology are damping systems[10–12], smart sensors[13] and microfluidic devices[14,15]. Among these, one of the recently emerged solutions is the use of magnetorheological elastomers (MREs), which consist of a soft elastomeric matrix filled with micron- or nano-sized magnetisable rigid particles. These magneto-responsive particles are generally classified as soft-magnetic and hard-magnetic particles. When soft-magnetic particles are used in an MRE, they can be magnetised by an external field. However, the magnetisation will disappear as soon as the external magnetic field is switched off. In the case of hard-magnetic particles, their magnetisation will largely remain even after the removal of the applied magnetic field. When designing such responsive materials, the choice of both (soft matrix and rigid particles) phases is crucial. In this regard, the stiffness of the polymeric matrix determines the composite resistance to deform under an external magnetic field, i.e., the softer the matrix, the stronger the magnetostriction response. Furthermore, the non-linear mechanical behaviour of the underlying matrix (i.e., strain hardening) determines the magnetorheological effect of the composite, i.e., the variation of material stiffness under magnetic actuation. Moreover, the choice of the magnetic particles defines the microstructural interactions and the nature of the magnetically induced stress transmission to the matrix. Generally, soft-magnetic particles are used to reach significant changes in material properties, whereas hard-magnetic particles are used to program geometrical actuation modes, i.e., shape-morphing features.

Experimental characterisations of both hard-magnetic MREs (hMREs) and soft-magnetic MREs (sMREs) have been extensively documented in the literature. These experimental investigations, on the one hand, are dedicated to understand the mechanical properties of both sMREs and hMREs through a wide range of deformation modes (e.g., uniaxial tension/compression, pure/simple shear and equi-biaxial tension) under mechanical and magneto-mechanical loadings[16–22]. On the other hand, pure rheological and magnetorheological tests have been conducted to understand the effects of magnetic actuation on various rheological properties, such as the change of their storage and loss moduli. For sMREs, the works of Stepanov et al.[23], Kallio[18], and Gordaninejad et al.[17] laid the foundations of a few experimental works that were conducted under a large mechanical stretching and coupled with the application of a magnetic field. In addition to the widely used uniaxial tensile and compression experiments, Schubert and Harrison[19,20] conducted a series of shear and equi-biaxial tensile tests on isotropic and anisotropic sMREs. Recently, Moreno et al.[24,25] reported a comprehensive experimental characterisation of extremely soft sMREs. For a review on experimental characterisations of sMREs, the paper of Bastola and Hossain[26] could be consulted. Note that although experimental studies of sMREs are available in the current literature, similar experimental characterisations for their hard-magnetic counterparts are quite limited at this point. Stepanov and co-workers[27–29] conducted some elementary mechanical and magneto-mechanical tests on hMREs while other recent works on these promising composites can be found in Antonel et al.[30], Kramarenko et al.[27], Koo et al.[31] and Moreno et al.[32].

Similar to the experimental investigations of sMRE and hMREs, mathematical modelling and numerical simulation to understand

[1]Department of Continuum Mechanics and Structural Analysis, Universidad Carlos III de Madrid, Avda. de la Universidad 30, 28911 Leganés, Madrid, Spain. [2]Zienkiewicz Centre for Computational Engineering, Faculty of Science and Engineering, Swansea University, SA1 8EN Swansea, UK. [3]Institute of Applied Mechanics, University of Erlangen-Nuremberg, Egerland Str. 5, Erlangen, Germany. [4]Glasgow Computational Engineering Centre, School of Engineering, University of Glasgow, G12 8QQ Glasgow, UK. ✉email: migmoren@ing.uc3m.es; danigarc@ing.uc3m.es

their underlying non-linear magneto-mechanically coupled behaviour have been an active field of research in the last years. Numerical frameworks help to further explore the full potential of MREs by facilitating the design and optimisation of multifunctional soft and flexible smart devices based on these fast-growing soft composites. MREs exhibit nonlinear and time-dependent behaviour in which the bulk elastomeric matrix shows incompressible characteristics[33–35] resulting in further complexities of their numerical simulations. The mathematical foundations of the coupling of electromagnetic fields at finite strains are well documented in some early publications, see for example the works of Pao[36], Eringen and Maugin[37], Maugin[38] and the references cited therein. More recent works related to the constitutive modelling for MREs are due to Ogden, Dorfmann, Bustamante, Shariff and co-workers[34,39–43]. While the aforementioned works discarded time-dependent phenomena of MREs, some works[44–53] considered time-dependent phenomena that are largely existing in the polymeric matrix. Note that the classical constitutive formulations of MREs that model the magneto-mechanical response at macroscopic levels clearly miss information of their underlying micro-structural composition. In contrast, multi-scale homogenisation-based methods directly transfer microscopic details of the MRE composition to the macroscopic scale. Despite the computational expense, homogenisation approaches provide more insights into the behaviour of MREs[51–64].

The great advances in both sMREs and hMREs to date pose a timely question on whether the combination of both types of particles may optimise the multifunctional response of these active structures. The macroscopic response of such hybrid MREs is not obvious as it results from complex interactions at the microscale. Some works in the literature provide manufacturing methodologies and some characterisation data on hybrid MREs[29,65–69]. However, a comprehensive characterisation of the magneto-mechanical behaviour of these materials and its dependency on the particle content is still missing. This is a fundamental question to motivate computational frameworks that would help to optimise and design functional applications. To this end, further experimental works are required to determine how the relative mixing ratio between soft- and hard particles modulates, in a combined fashion, both material property changes and shape actuation modes. To the best of the authors' knowledge, there are only a few works approaching this problem. Sanchez and co-authors[70] addressed the analysis from a molecular dynamics basis and, more recently, Becker and co-authors[71] proposed a mesoscopic constitutive model. Although the later work definitely provided relevant observations, it was performed under the assumption that the elastomeric matrix was rigid. Therefore, there is still a big gap of knowledge on how soft hybrid MREs perform under different magneto-mechanical conditions and the identification of the microstructural mechanisms governing such a behaviour.

In this work, we aim at filling the current gap of knowledge providing a complete magneto-mechanical perspective on extremely soft hybrid MREs. To this end, we manufactured MRE samples considering different mixing ratios between soft- and hard-magnetic particles. The elastomeric matrix chosen presents a material stiffness in the order of 1 kPa, so that significant magnetorheological effects can be reached even for very low external magnetic fields. At first, a comprehensive experimental characterisation was performed providing tests under oscillatory shear, frequency sweeps and axially confined mechanical conditions while applying different external magnetic amplitudes. The results show that the choice of an adequate mixing ratio between soft- and hard-magnetic particles allows to optimise the magneto-mechanical performance of MREs. As the experimental data relies on the macroscopic realm, it is difficult to get insights into the microstructural mechanisms. To overcome this issue, we developed a computational framework that serves as a numerical testbed for the evaluation of the magnetic interactions between particles and their influence on the mechanical response of the composite. The framework is based on a full-field computational model that explicitly accounts for the different phases, i.e., elastomeric matrix, soft- and hard-magnetic particles. The numerical results suggest that soft-magnetic particles are responsible for amplifying the magnetic field, whereas hard-magnetic particles are the main driver in torsion-driven actuations. The experimental insights were then accounted for the numerical design of different micro-beams that offer alternative actuation modes. Such structures allow either for bending actuation or the increase in mechanical properties (e.g., stiffness) depending on the direction of the external magnetic field. The latter was achieved thanks to the multifunctional coupling that the combination of both soft- and hard-magnetic particles provides. Overall, the experimental and computational results complement each other to provide a complete view of the magneto-mechanical coupling in hybrid MREs across scales.

RESULTS

Soft-hard particles ratio optimises the response of hybrid MRE

Results available in the literature have shown that MREs embedding soft-magnetic particles can present significant increases in the material stiffness under external magnetic actuation. Along with such changes in the material properties, sMREs undergo remarkable mechanical deformations, mainly along the applied magnetic direction. Due to the negligible magnetic hysteresis of the soft-magnetic particles, these changes are not sustained when the external magnetic field is switched off. On the contrary, hMREs usually show smaller changes in stiffness but can present high and complex shape-morphing phenomena. Due to the dissipative behaviour of hard-magnetic particles and their capability to acquire remanent magnetisation, material property changes can be partially sustained even in the absence of external magnetic actuation.

In the present work, we perform magnetorheological tests to explore how the combination of both soft- and hard-magnetic particles modulates the individual features of sMREs and hMREs within a hybrid sample. To this end, we manufacture extremely soft composites with three phases: an elastomeric matrix of very low stiffness (≈1 kPa), soft-magnetic particles and hard-magnetic particles, with different volumetric ratios between both types of particles, understood hereafter as soft-to-hard particles ratio. For more details on the material data and manufacturing methods, see Methods and Supplementary Methods 1. The experiments were conducted in a magneto-mechanical rheometer on two types of samples: (1) virgin samples, i.e., specimens that have not been exposed to any external magnetic field; and (2) pre-magnetised samples, i.e., specimens exposed to an axial magnetic field of 1 T. The results are collected in Fig. 1. More details on the testing methods and related results are provided in Methods and in Supplementary Discussion 1.

Figure 1a–c shows hysteresis loops (Lissajous figures) of the evolution of the shear stress with respect to the shear strain. Figure 1d synthesises the results as plots of the maximum shear stress against the external magnetic field. It compares the response for all the soft-to-hard-magnetic mixing ratios (including the extreme cases of pure soft- and hard-magnetic MREs) and for virgin and pre-magnetised samples. These results indicate that the magnetorheological stiffening increases with the amount of soft-magnetic particles. While maximum stresses of 26 kPa are reached in sMREs under 1000 mT, only a maximum of 5 kPa is reached in hMREs. In this regard, hybrid MREs stand in the middle with values of 21, 15 and 13 kPa for mixing ratios of 2:1, 1:1 and 1:2, respectively.

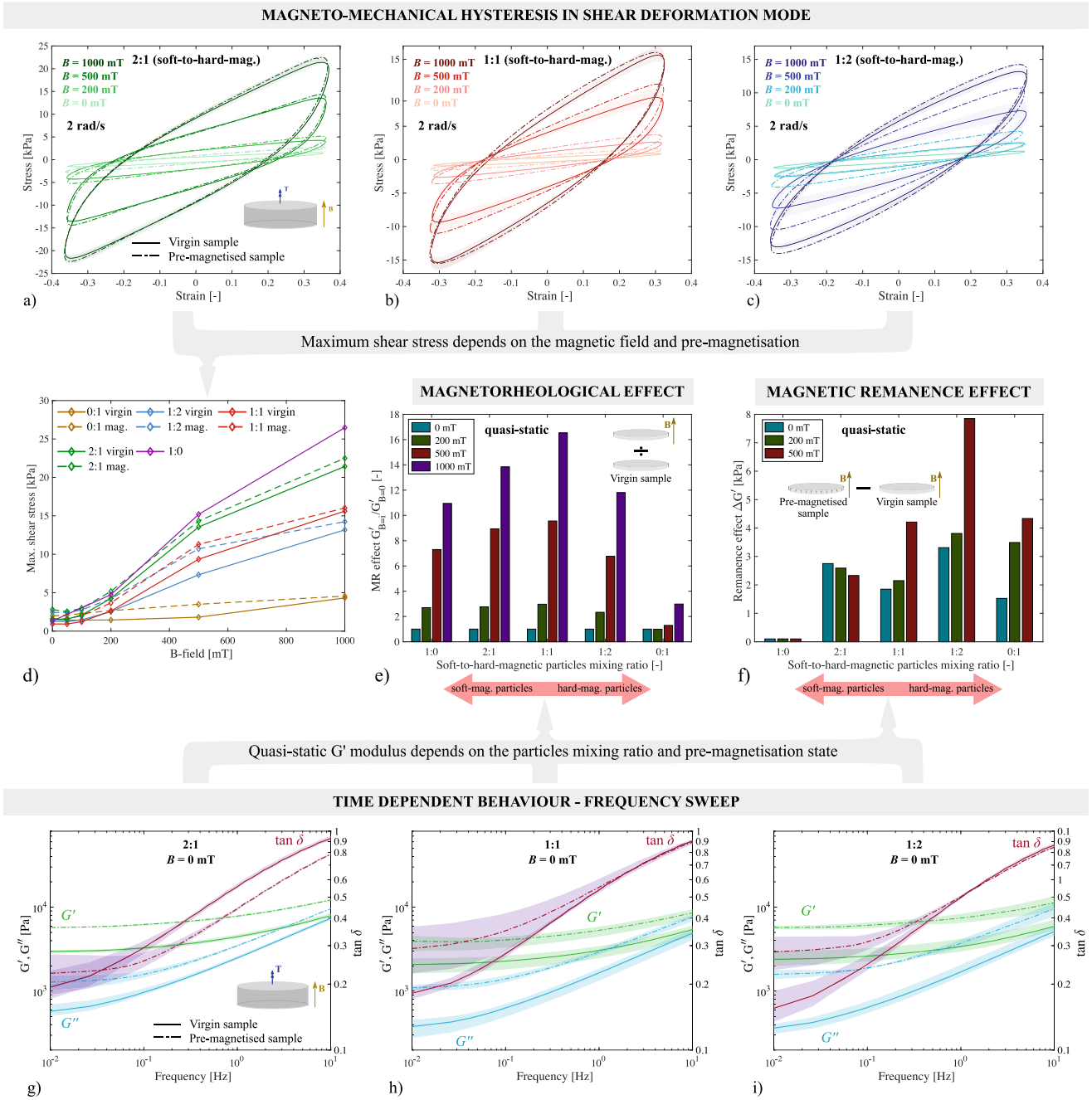

Fig. 1 Experimental characterisation of the magnetorheological and magnetic remanence effects depending on the mixing ratio between soft- and hard-magnetic particles. Results from constant oscillatory shear loops for soft-to-hard-magnetic particles mixing ratios of **a** 2:1, **b** 1:1 and **c** 1:2. The total amount of particles is 30 vol.%. The experiments are performed on both virgin and pre-magnetised samples (i.e., previously exposed to 1000 mT axial magnetic field). **d** Maximum shear stress reached during the constant oscillatory shear tests depending on the magnetic field applied, and for different particles' mixing ratios. The solid lines denote experimental results on virgin samples and dashed lines denote experimental results on pre-magnetised samples. **e** Magnetorheological effect, i.e., the ratio between the storage shear moduli under magnetic actuation and under null magnetic actuation, for different hybrid MREs. **d** Magnetic remanence effect, i.e., the difference between the storage shear moduli of pre-magnetised and virgin samples, for different hybrid MREs and different applied magnetic fields. **g**–**i** Frequency sweep tests under shear loading and null magnetic actuation on virgin (solid lines) and pre-magnetised (dash lines) hybrid MREs with mixing ratios of 2:1, 1:1 and 1:2, respectively. These results are presented in terms of storage (G') and loss (G'') moduli, and loss factor ($\tan\delta$).

Frequency sweep tests under shear loading and different external magnetic conditions provide insights into the rate-dependent behaviour of MREs (Fig. 1g–i). Supplementary Discussion 1 contains the results for the frequency sweeps under a magnetic actuation. All samples, irrespective of the particle mixing ratio or magnetic field applied, present a stiffening response with the strain rate (i.e., frequency here). This owes to the viscoelastic nature of the elastomeric matrix. In addition, all samples present a clear magnetorheological stiffening with the applied magnetic field. Regarding this last point, we collect the corresponding data in Fig. 1e. Here, the magnetorheological effect is defined as the ratio between the storage shear moduli under magnetic actuation

and under null magnetic actuation. As expected, sMREs present much higher effects than hMREs due to the higher relative magnetic permeability and the subsequent more intense particle magnetic interactions. However, surprisingly, the maximum magnetorheological effect is found for a soft-to-hard particle ratio of 1:1. These results suggest that the combination of soft- and hard-magnetic particles enhances the effective magnetic field within an MRE and increases the magnitude of the dipole-to-dipole magnetic interactions. In this regard, the reader may note that internal forces between particles not only depend on their magnetisation (higher in the soft particles) but also on their volume (larger for the hard particles).

Moreover, Fig. 1g–i shows the results for null magnetic actuation on virgin (solid lines) and pre-magnetised (dashed lines) hybrid MREs. These results unveil remarkable differences in terms of storage (G') and loss (G'') moduli between virgin and pre-magnetised samples. To elaborate on this, the magnetic remanence effect, understood as the magnetorheological stiffening sustained after removing the magnetic field, is demonstrated in Fig. 1f. As expected, pure sMREs do not present any remanence effect due to the low magnetic coercivity of the soft-magnetic particles. One would expect such a remanence effect to be maximum for pure hMREs. However, the results indicate that the maximum corresponds to hybrid MREs with a mixing ratio of 1:2. This observation can be explained by the interaction between soft- and hard-magnetic particles during and after the pre-magnetisation processes. In this regard, during the pre-magnetisation, the externally applied field of 1000 mT is internally amplified by the soft-magnetic particles, favoured by their high relative magnetic permeability (30 times higher than in hard-magnetic particles). Such an amplified magnetic field promotes a higher remanent magnetisation in the hard-magnetic particles. Moreover, when the external field is switched off, the hard particles sustain residual magnetisation. Due to dipole-to-dipole interactions, this magnetisation influences the surrounding soft particles forming magnetic bridges. The magnetic field generated by the hard particles is amplified by the soft ones, thus enhancing the interactions between particles at the microscale. These interactions create a higher resistance of the composite to deform, resulting in a remanent stiffening effect.

The magnetic stress is modulated by soft-hard particles ratio

Under the application of an external magnetic field, MREs respond mechanically by deforming and/or changing their mechanical and rheological properties. This behaviour is the result of balancing the pure mechanical stresses and magnetically induced stresses within the sample. The former are related to the passive deformation of the material and the mechanical properties of both elastomeric matrix and particles. They can be easily measured by a traditional experimental testing. The latter stresses relate to magnetic particle interactions at the microstructural level. Such interactions result in attractive and repulsive forces that contribute to macroscopic deformations. Although these interactions are difficult to analyse experimentally, we evaluate them from the macroscopic magnetic stress induced in the MRE samples. This stress state is an excellent indicator of the physics governing internal processes as it is the direct result of microstructural interplays within the composite.

To conduct the experiments, we used the magneto-mechanical rheometer to provide mechanically confined studies. The magnetic actuation leads to particles interactions within the sample that produce a macroscopically confined expansion. The system measures the axial force due to the unique contribution of magnetic stresses. The tests were conducted on virgin and pre-magnetised samples and under two different actuation modes: (i) direct actuation, i.e., applying the magnetic field in the same direction as the pre-magnetisation; and (ii) reverse actuation, i.e., applying the magnetic field in the opposite direction to the pre-magnetisation. More details on the testing methods are provided in Methods. Figure 2a, b2 shows these results for sMREs and hMREs, respectively; and Fig. 2c2, d2, e2, for the different hybrid MREs tested.

The response of sMREs is found to be independent of the direction of the applied magnetic field, and shows strong magnetically induced stresses. This can be explained by their low magnetic coercivity, which allows them to magnetise in the direction of the applied magnetic field without sustaining significant remanent fields. The larger stresses with respect to hybrid and hMREs may be explained by the higher magnetic permeability of soft-magnetic particles that enhances particles interactions. On the contrary, hMREs present lower induced stresses but their overall response highly differs for direct to reverse actuation. This is explained by the residual magnetisation of the hard particles. Under a direct actuation, they tend to form chain-like structures leading to the expansion of the sample. For a reverse actuation, however, they tend to rotate and compress the sample. Regarding the response of hybrid MREs, it seems clear that the presence of soft particles is the main modulator under these conditions, tending all these samples to expand irrespective of the actuation mode (direct or reverse). In addition, the maximum stresses induced directly correlate with the number of soft particles, i.e., 22, 18 and 15 kPa for mixing ratios of 2:1, 1:1 and 1:2, respectively. Under confined conditions, the effect of the hard particles in the hybrid MREs can be noted by a jump in the maximum stresses for direct and reverse actuation modes. Although the experimental results (Figs. 1 and 2) suggest some interesting synergistic effects and complex interactions between soft- and hard-magnetic particles at the microscale, the study is restricted to macroscopic observations. In the following, we overcome this limitation by developing a virtual testing framework to analyse such microstructural responses.

Microstructural computational model for hybrid MREs

The experimental results of hybrid MREs demonstrate a macroscopic stiffening of these materials under the application of external magnetic fields (Fig. 1). From the mechanically confined tests in Fig. 2, we show that such a magneto-mechanical coupling is the result of internal stresses derived from the interactions between soft- and hard-magnetic particles that are, in turn, transmitted through the elastomeric matrix. These interactions are of high complexity due to strong contrasts in the material properties of the different phases. Regarding the mechanical problem, there is an important stiffness contrast between the matrix (kPa) and particles (GPa). Moreover, the magnetic problem also presents an important phase contrast in terms of the relative magnetic permeability, which presents a value close to 1 for the matrix and hard particles whereas in the soft particles it is 31. These characteristics make the understanding of the problem non-intuitive, limiting the analysis to macrostructural measurements and hindering the identification of the links at the microscale.

We develop a magneto-mechanical finite element (FE) model to provide a virtual testing framework to analyse the interplays between the hybrid MRE phases at the microscale. The computational framework, presented in Methods, formulates the magneto-mechanical problem at finite deformations and considers the elastomeric matrix as an incompressible material. The model parameters have a clear physical meaning and their values are directly taken either from the experiments presented herein or from the literature. More details on the constitutive formulation, the material parameters, the homogenisation framework and boundary conditions are provided in Supplementary Methods 2–4.

The computational model allows to link macroscopic measurements with material properties of the phases at the microscale. In

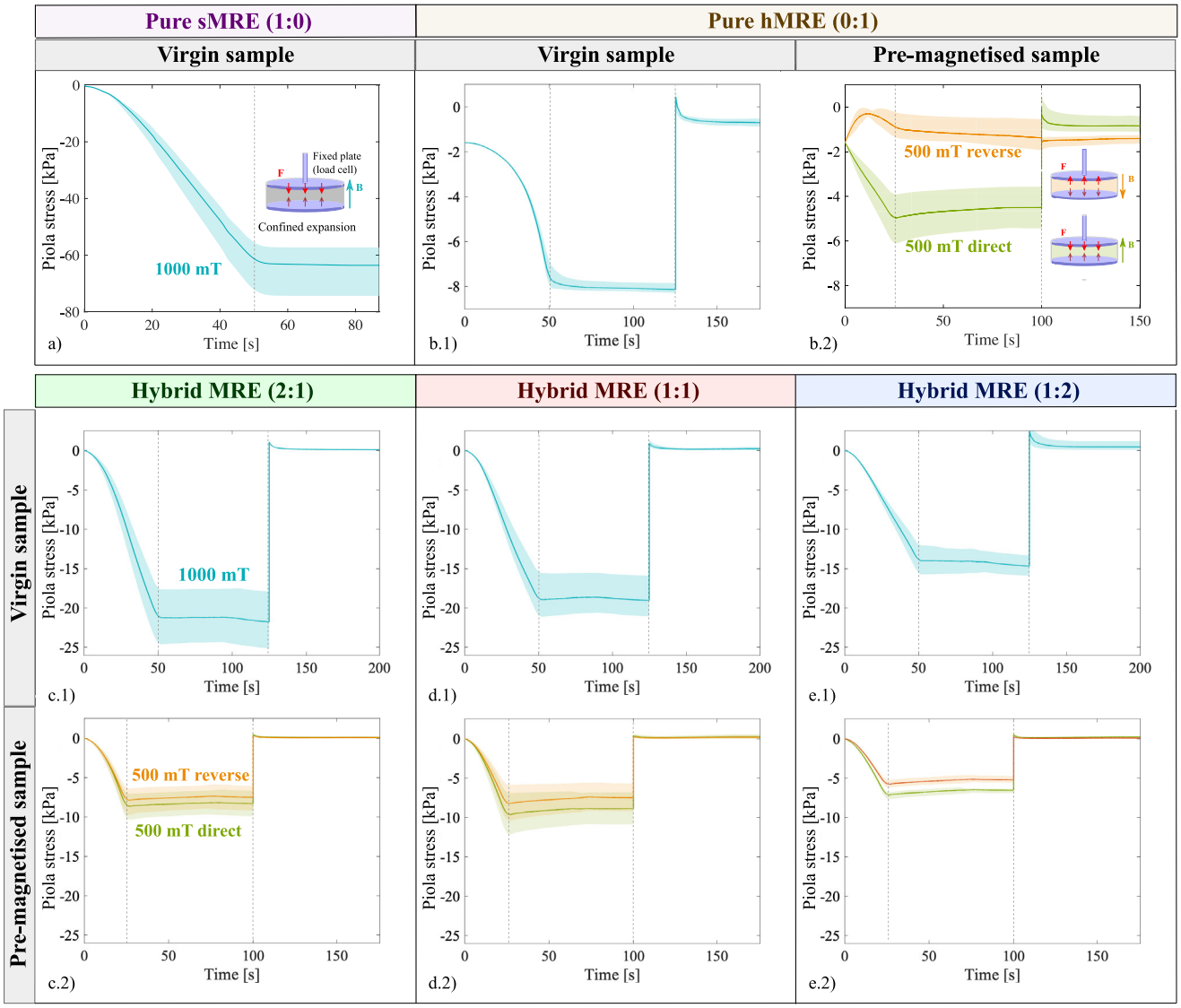

Fig. 2 Macrostructural evaluation of microstructural magneto-mechanical interactions. Time evolution of the axial stress (Piola stress) exerted by mechanically confined samples on the upper plate of the rheometer for multiple soft-to-hard-magnetic particles mixing ratios of **a** 1:0, **b** 0:1, **c** 2:1, **d** 1:1, **e** 1:2. The experiments are conducted on virgin and pre-magnetised samples. The magnetic field on virgin samples is applied until reaching a maximum of 1000 mT, then kept constant for 75 s and finally switched off. On the pre-magnetised samples, the experiments include direct and reverse magnetic actuation following the same procedure but limiting the actuating magnetic field up to 500 mT.

this regard, a crucial parameter is the residual magnetisation at the single-particle level, defined by the variable $\mathbb{H}_r$. The evaluation of this variable is experimentally unapproachable, being limited to macroscopic measurements of the apparent magnetic remanence (i.e., using a Teslameter on the pre-magnetised samples). However, the computational framework developed herein allows to estimate the residual magnetisation of the hard particles that leads to an experimental macroscopic value. With an experimental measure of the residual macroscopic magnetic induction in pre-magnetised hMRE samples, an inverse engineering approach searches for the value of $\mathbb{H}_r$ in the hard particles. The apparent $\mathbb{B}$ and $\mathbb{M}$ fields obtained are shown in Supplementary Fig. 3. The reader can also see Supplementary Methods 6 for more detail on this calibration procedure.

In the magneto-mechanical experiments, the extremely soft nature of the polymeric matrix allows the magnetic particles to rearrange forming chain-like structures within the MRE (see discussion for sMREs in ref. [24]). These deformation mechanisms imply very large deformations within the MRE that are not computationally reachable due to excessive element distortions. This fact, together with the need for explicitly simulating the magnetic sources, hinders a direct comparison between the experimental and computational results. However, the computational model enables simulating at the microscale, within a homogenisation framework, the magneto-mechanical interactions between soft and hard particles depending on their mixing ratio. The simulations help to explore the nature of such interactions and the main microstructural deformation mechanisms transmitted to the matrix. To this end, we first applied the permanent magnetisation of the hard-magnetic particles (positive along *z*-axis by the imposition of the variable $\mathbb{H}_r$). Then, a second step applied an Eulerian (homogenised) magnetic induction up to 10 mT in the same direction as the magnetisation (i.e., direct magnetic field) and in the opposite direction (i.e., reverse field). It is important to note that while in the experiments we analysed the response of the macroscopic sample to an externally applied magnetic field,

here we directly prescribed a homogenised magnetic field within the RVE. Thus, the computational framework allows to explore the intrinsic material behaviour and microstructural interactions for such prescribed magnetic fields that are the result of external magnetic sources, residual magnetisation in the hard particles and evolving fields within the soft particles. In other words, a null magnetic field in the RVE does not mean null external stimulation but an externally applied magnetic field that balances the residual magnetisation within the RVE. We find this approach ideal for the purpose of these simulations, which is to evaluate the interactions between particles on a macroscopically constrained RVE. In addition, setting a common homogeneous magnetic induction to zero for all the RVEs and mixing ratios makes it possible to compare the response between all of them. More details about the boundary conditions and the residual homogeneous magnetic induction after pre-magnetisation can be found in Supplementary Methods 4 and 6.

Pre-magnetised hybrid MREs perform differently depending on the direction of the magnetic actuation. The computational results from the simulations are presented in Fig. 3. The first column depicts representative RVEs for each soft-to-hard particle ratio. The second column presents plots of the homogenised stress in the RVEs against the homogenised magnetic field for direct and reverse actuations. Five different RVEs for each MRE type allow to characterise the variability related to the random distribution of the particles. Associated with these results, the last column shows the magnitude of the magnetic field for both direct and reverse actuations under a macroscopic field of 5 mT. As previously stated, note that we prescribe the total macroscopic magnetic induction. Finally, we noticed that some simulations face convergence issues as the particles approach each other and try to form chains. These phenomena depend on the distances between particles and their soft or hard nature.

A first finding relates to the response of the MREs under direct and reverse actuations. In this regard, sMREs present exactly the same behaviour irrespective of the direction of the external field, whereas the response of the hybrid and hMREs strongly differs depending on the direction of the magnetic actuation. The remanent magnetisation of the hard-magnetic particles explains such a behaviour. For sMREs, the particles magnetise along the applied magnetic direction leading to dipole-to-dipole interactions and a subsequent compression of the RVE. If larger magnetic fields are applied, the extremely soft matrix would allow the particles to rearrange forming chain-like structures. On the contrary, the residual magnetisation within the hard-magnetic particles adds magnetic torques. These torques appear when the magnetisation is not perfectly aligned with the external field. From the magnetic point of view, under direct magnetic fields, the magnetisation within the hard particles is reinforced. However, for reverse fields, the total magnetisation in the hard particles is diminished due to balancing between energetic and residual terms in such a direction. In addition, the higher permeability of the soft particles results in a higher magnetisation than for hard particles. The mixing of both types of particles leads to synergistic effects. In this case, as can be observed in Fig. 3 from the magnetic field representations, the soft particles create magnetic bridges between the hard ones, a phenomenon that amplifies the magnetisation and enhances the magneto-mechanical coupling. This latter observation may explain the better performance of the hybrid MREs observed in the experiments. The following section will elaborate on these phenomena.

Regarding the values of the magnetic field, and for, e.g., a macroscopic magnetic induction of 5 mT, we observe larger local fields of 20 mT in the soft magnetic particles, whereas the saturation magnetisation is 2.5 T. Despite this fact, the extremely soft nature of the elastomeric matrix leads to significant macroscopic mechanical performance for magnetic fields in that range. Furthermore, when prescribing reverse magnetic actuation, the magneto-mechanical coupling is even stronger, which translates into a larger induced macroscopic stress. Moreover, the results from pure hMRE simulations (hMRE (0:1)) reach higher macroscopic inductions of up to 100 mT. The analysis of the results shows finite local deformations and high microstructural magnetic gradients. This provides insightful observations of the microstructural mechanisms that are influencing the macroscopic response of the MREs experimentally tested.

A further factor determining the mechanical behaviour of hybrid MREs is the relative size ratio between soft- and hard-magnetic particles. In this regard, and in addition to the previous results, we have conducted further simulations to understand how differences in the relative size between particles affect the microstructural magneto-mechanical coupling. To this end, we performed simulations on RVEs of hybrid MREs with a soft-to-hard-magnetic particles' mixing ratio of 1:1. Then, different particles size ratios (soft:hard) were considered: 6:1, 3:1, 1:1, 1:3, 1:6 (see Supplementary Discussion 2). These results suggest a stronger magneto-mechanical coupling when using soft-magnetic particles smaller than the hard-magnetic ones. The effect is clearer when applying a reverse magnetic field (i.e., contrary to the initial magnetisation direction). The bigger size of the hard-magnetic particles favours the transmission of the magnetic torque, whereas a lower size of the soft-magnetic particles contributes to generate magnetic bridges between the hard particles leading to synergistic effects. On the contrary, i.e., smaller hard-magnetic particles, the magnetic bounding between the big soft particles is much weaker and the overall magneto-mechanical coupling becomes smaller.

Virtual testing framework to design multifunctional actuators

The previous experimental and numerical results suggest the possibility of mixing soft- and hard-magnetic particles to provide, at once, superior bending deformations and material stiffness enhancements under magnetic actuations. Recent advances in additive manufacturing (3D printing) techniques have made possible the design of micron-size actuators based on MREs[72–75]. Ideally, the use of an extremely soft elastomeric matrix, as in this work, allows for magnetic stimulation with very low fields. These materials and micron-size structures have the potential to open new routes for the soft robotics community. However, the conceptualisation and design of such systems present significant difficulties. For instance, the lack of proper experimental methods hinders the evaluation of magneto-mechanical coupling at this scale. In this section, we aim at demonstrating the capacity of the presented FE model as a virtual testing framework to overcome the bottlenecks impeding this advance. To this end, we design two micron-sized beams (homogeneous and bimorph) that, depending on the direction of a low actuating magnetic field (below 50 mT), react either by deflecting or by performing functional changes in their material properties, i.e., significant stiffening.

We have developed a FE model consisting of a beam surrounded by air, see Fig. 4 for the case of a bimorph (i.e., bi-layered beam). The constitutive model of the beam layers relies on the microstructural description of the phases, i.e., matrix and particles. The top layer of the beam corresponds to a MRE component while the bottom layer is a purely elastomeric matrix. Details on the numerical implementation are presented in Methods. Moreover, the reader can find in Supplementary Discussion 3 the results for a homogeneous beam with the particles scattered along the matrix.

The main outcome is that, under a perpendicular magnetic actuation, the rightwards pre-magnetised hard particles lead to the bending of the beam. Indeed, the transmission of torques from the particles to the matrix governs such a functional mechanism. Moreover, soft particles enhance the torques on hard

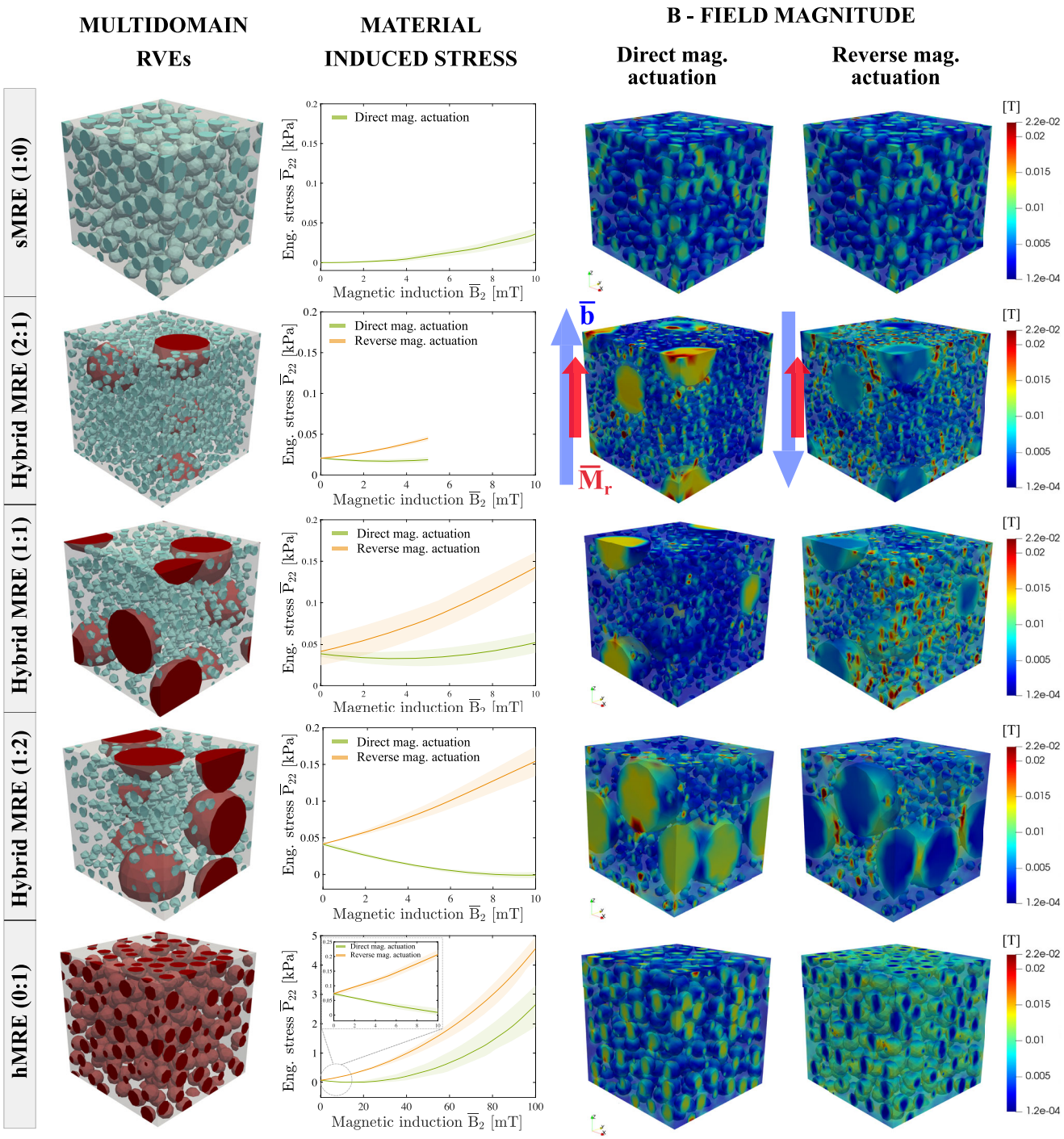

Fig. 3 Computational results of the microstructural magneto-mechanical coupling using a homogenisation model. Computational results for the homogenised framework when subjecting different representative volume elements (RVEs) to homogeneous magnetic inductions while applying mechanical confinement. The first column shows representative RVEs for the different particle mixing ratios analysed. The second column presents the homogenised stress against the prescribed homogenised magnetic induction for direct and reverse actuations. The last column shows the microstructural distribution of the magnetic induction within the RVEs for direct and reverse actuation for a macroscopic Eulerian magnetic induction of 5 mT. Note that a scheme with two collinear arrows illustrates the directions of the prescribed magnetic induction (blue) and permanent magnetisation (red) vectors for direct and reverse magnetic actuation. In addition, five RVEs have been considered for each particle mixing ratio. The stress versus magnetic induction curves include scatter areas to quantify the numerical variability. Also, note that a representative RVE has been chosen for each mixing ratio in the magnetic induction plots.

ones in two ways: (i) amplifying the magnetic field around the hard particles and (ii) compressing the upper layer along the beam thickness. Regarding the former, the soft-magnetic particles, with a high magnetic permeability, create magnetic pathways around the hard-magnetic particles. Such a phenomenon increases the effective magnetic flux, which directly impacts the resultant microscopic torque transmitted from the hard particles to the matrix. Note that such magnetic pathways appear not only in the perpendicular (vertical) direction, but also in the longitudinal (horizontal) direction. Figure 4.f2 clarifies this phenomenon. After

the initial pre-magnetisation, the homogeneous longitudinal magnetisation slightly increases with the perpendicular magnetic actuation, contrary to the behaviour of the pure hard-magnetic beam in Fig. 5.f3. Regarding the latter, soft particles magnetise in the perpendicular direction, with the consequent dipole-to-dipole interactions and the perpendicular compression of the layer. With this contraction, the upper layer expands, thus the structure bends. These features can be appreciated in Fig. 4d. In addition, Fig. 4f depicts the evolution of the homogeneous magnetisation of the hard, soft and hybrid beams in both perpendicular and parallel directions.

The reader interested in additional results of the bimorph beam pre-magnetised in the opposite direction, i.e., leftwards pre-magnetisation, is referred to Supplementary Fig. 6. Moreover, Supplementary Fig. 9 shows additional results for the pure hard-magnetic bimorph under a larger magnetic actuation of 200 mT. This allows to see high local torsional deformations of the matrix in the particles' vicinity, which owes to the extremely soft nature

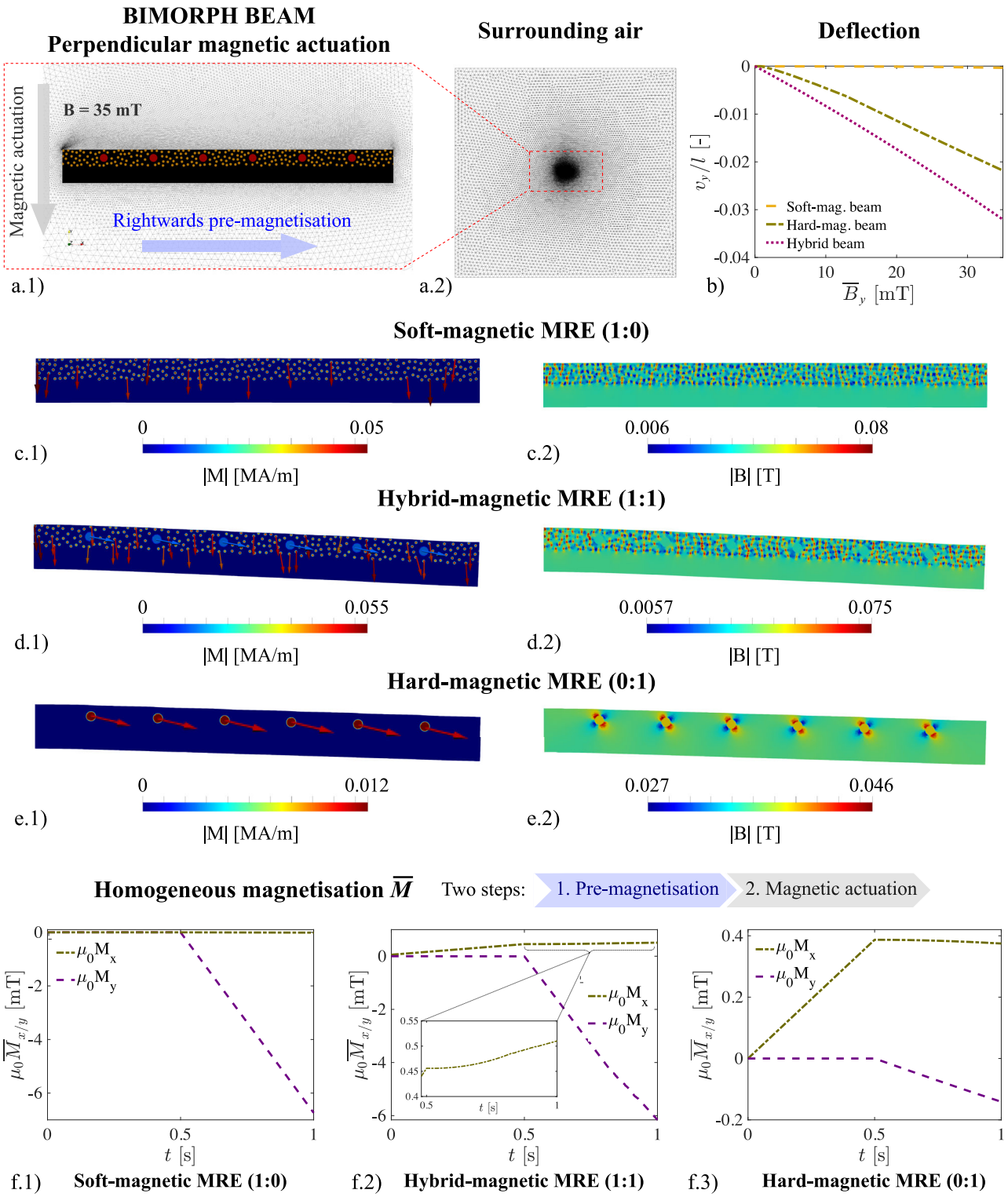

Fig. 4 Numerical application of the microscopic model on a bimorph cantilever beam. a.1 Perpendicular magnetic actuation condition on a bi-layer cantilever beam with hybrid magnetic fillers (soft- and hard-magnetic particles) in the top layer and pure elastomeric matrix in the bottom layer. **a.2** Complete FE problem mesh including the air surrounding the beam to guarantee the proper application of the magnetic actuating field. **b** Normalised beam deflection against the external applied magnetic field depending on the filler content used in the upper layer: sMRE, 1:1 hybrid MRE and hMRE. The hMRE beam and the hybrid beam bend under an external magnetic actuation as a consequence of the torque transmission from the hard-magnetic particles. The *z*-deflection is normalised by the length of the beam. **c.1**, c.2 Magnetisation and magnetic induction fields within the sMRE beam after magnetic actuation (35 mT), respectively. **d.1**, **d.2** Magnetisation and magnetic induction fields within the hybrid MRE beam after the magnetic actuation (35 mT), respectively. **e.1**, e.2 Magnetisation and magnetic induction fields within the hMRE beam after magnetic actuation (35 mT), respectively. **f.1–3** Evolution of the homogenised horizontal and vertical magnetisation components of the sMRE, hybrid MRE and hMRE beams, respectively. In these simulations, a pre-magnetisation step is applied first, followed by the magnetic actuation. Note that the arrows on the particles describe the Eulerian magnetization vector at their centres.

of the matrix and explains the non-perfect parabolic macroscopic structural bending.

A completely different response is expected when the magnetic actuation is parallel to the beam. For low external magnetic fields (25 mT), the hybrid MRE beam responds by increasing its apparent stiffness. Note that small enough fields prevent significant structural compression in the presence of soft particles, while being sufficient to functionally activate the structure. Figure 5 shows the results of these simulations. After the application of a parallel magnetic field on the pre-magnetised beam, a small stretch is applied in the same longitudinal direction. The apparent stiffness is computed as the homogenised axial Piola stress over the equivalent strain. In addition to the bimorph cantilever beam, Fig. 5 includes the results for a homogeneous beam, i.e., particles scattered along all the matrix. This allows to directly compare the magneto-mechanical stiffening of both beams and extract insightful information.

A glance over the results from Figs. 4 and 5 shows that the use of hybrid MREs enables multi-actuation modes with a single structure. Note that we added the response of pure sMRE and hMRE beams in Figs. 4 and 5. The hMRE provides bending actuation but almost negligible stiffening at low magnetic fields. On the contrary, the sMRE provides outstanding stiffening under applied magnetic fields but a negligible bending. Our proposed solution, i.e., hybrid MREs, provides an enhanced bending actuation beyond that of hMREs, whereas it keeps a similar material stiffening to that of sMREs for a low magnetic actuation. The results for the homogeneous beam in Fig. 5g indicate that the hybrid MRE beam provides a stronger stiffening effect than the pure sMRE and hMRE ones. These numerical results are supported by the experimental findings in Fig. 1e, which suggest the possibility of using hybrid MREs to combine enhanced mechanical actuation and change in the material properties.

DISCUSSION

sMREs undergo remarkable stiffening under a magnetic actuation, while hMREs perform intricate morphological changes. Our experimental approach demonstrates that hybrid MREs combining both soft- and hard-magnetic particles exhibit both functional behaviours. In addition, the use of an extremely soft elastomeric matrix allows the activation of such couplings even with very low magnetic fields. To uncover the microstructural mechanisms that govern the multifunctional behaviour, we developed a FE-based homogenisation framework. The attributes of the hybrid MREs and enhanced magneto-mechanical coupling open new routes for the conceptualisation and design of soft robots, microfluidic devices and bioengineering applications. In this regard, we extended the computational framework to provide a virtual testing platform that facilitates the design of such applications. It can evaluate the mechanical response of micron-size actuators accounting for the mixing ratio and distribution of the soft and hard particles within the polymeric matrix.

Making use of this computational tool, we designed a bi-layer beam (bimorph actuator) that provides enhanced morphological changes and functional changes in its mechanical properties (material stiffness) depending on the relative direction of the external magnetic field. This application may be useful in, for example, microfluidic systems to actuate in two modes. The beam bending can be activated via a perpendicular magnetic stimulation and a parallel fluid flow can be penalised. Alternatively, the parallel magnetic stimulation would increase its structural stiffness opposing to the fluid flow perpendicular to the beam. Another application area with great potential is bioengineering. The current hybrid MRE solutions are ideal candidates to push the advance in mechanobiological systems based on magneto-active polymers, as the recent work published by the authors[32].

Moreover, the results for a homogeneous beam with the particles scattered along all the matrices confirm the experimental findings. The hybrid MRE actuator presents enhanced material stiffening with respect to the pure sMRE and hMRE counterparts. While the sMRE and hMRE stiffen 2.9 and 1.1 times with the magnetic field, respectively, the hybrid MRE stiffens 4.2 times. That makes the stiffening of the hybrid MRE almost 150% larger than that of pure sMREs. Such a finding is the result of the amplification effect of the local magnetic field due to the pre-magnetised hard particles surrounded by highly magnetisable soft particles. Even though this effect is less clear for the bi-layer actuator, it is still beneficial as its deflection under perpendicular magnetic actuation is larger than the pure sMRE and hMRE ones.

Another potential application of the bi-layer beam is to provide the same actuation mode independently of the external magnetic source. In this regard, sometimes it is difficult to control a specific magnetic field direction. However, under high enough magnetic fields, our bi-layer beam would deflect for both perpendicular and parallel actuations. A perpendicular field would activate the torques from the hard-magnetic particles, whereas a parallel field would activate compression/tensile deformation in the upper layer due to dipole-to-dipole interactions mainly arising from the soft particles. The axial deformation of the upper layer, in the presence of the lower passive layer, would also induce a mechanical bending.

Overall, this work provides the experimental and computational bases to design multifunctional structures with a high flexibility from different perspectives. First, the softness of the elastomeric matrix facilitates the magnetic stimulation, as the actuation modes can be activated with very low fields (<50 mT). In addition, it offers flexibility in the manufacturing process allowing to mix micron-size magnetic particles with six-times difference in size and different relative permeability and coercivity. Therefore, it opens great possibilities for the design of materials with different apparent relative magnetic permeability, viscosity, and stiffness. The magneto-mechanical coupling can also be modulated by choosing either another elastomeric matrix with different stiffness, or changing the size, coercivity and magnetisation saturation of the particles. In addition, these hybrid MREs have been manufactured by homogeneously distributing

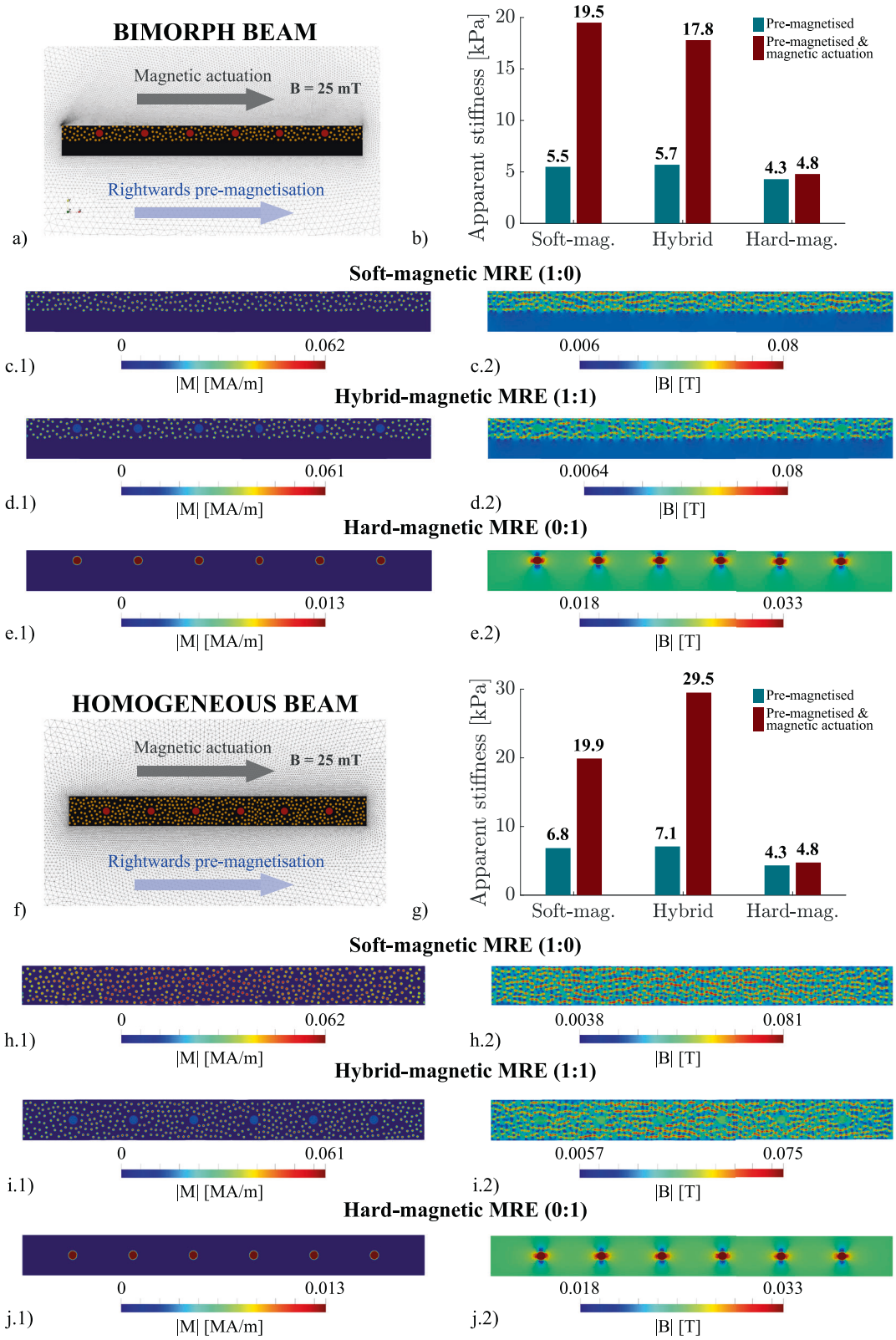

the particles within the elastomeric phase. Alternatively, small magnetic fields could be imposed during the curing process to allow for the formation of chain-like particles structures leading to anisotropic properties and opening other actuation possibilities. In general terms, the most important flexibility provided by these structures is the multi-actuation modes. As shown in our virtual demonstration, these permit for changes in both shape and material properties. In addition, it opens other possibilities such as functionally graded materials to activate locally different actuation modes.

Fig. 5 Numerical application of the microscopic model on a bimorph and homogeneous cantilever beams. a Parallel magnetic actuation condition on a bi-layer cantilever beam with hybrid magnetic fillers (soft- and hard-magnetic particles) in the top layer and a pure elastomeric matrix in the bottom layer. **b** Apparent stiffness of the bimorph beam after pre-magnetisation under null and magnetic actuations of 25 mT, depending on the filler content used in the upper layer: sMRE, 1:1 hybrid MRE and hMRE. **c.1**, **c.2** Magnetisation and magnetic induction fields within the sMRE beam after the magnetic actuation (25 mT), respectively. **d.1**, **d.2** Magnetisation and magnetic induction fields within the hybrid MRE beam after the magnetic actuation (25 mT), respectively. **e.1**, **e.2** Magnetisation and magnetic induction fields within the hMRE beam after magnetic actuation (25 mT), respectively. **f** Parallel magnetic actuation condition on a homogeneous cantilever beam with the particles scattered along all the matrix. **g** Apparent stiffness of the homogeneous beam after the pre-magnetisation under null and magnetic actuation of 25 mT, depending on the filler content used in the upper layer: sMRE, 1:1 hybrid MRE and hMRE. **h.1**, **h.2**, **i.1**, **i.2**, **j.1**, **j.2** Magnetisation and magnetic induction fields within the sMRE, hybrid MRE and hMRE beams, respectively, after the magnetic actuation.

The combination of the experimental and computational methods developed herein would make possible the conceptualisation of composite structures with superior performance. To this end, the microstructural modelling framework could be used to generate a large database considering different material properties for each phase (i.e., elastomeric matrix, soft and hard magnetic particles), differences in particle size, alternative microstructural arrangements of the particles, etc. Then, the optimal solutions from a microstructural perspective could be obtained from such algorithms and tested experimentally to validate a superior multifunctional performance at the macrostructural level. The latter would benefit from machine learning or Bayesian optimisation methods[76–78].

METHODS

Materials and synthesis

We manufacture extremely soft composites with three phases: an elastomeric matrix of very low stiffness (≈1 kPa), soft-magnetic particles with a mean diameter of 5 μm, and hard-magnetic particles with a mean diameter of 30 μm. For the matrix, an extremely soft elastomer Dowsil CY52-276 (DowSil, Midland, MI, USA) (PDMS with stiffness below 10 kPa) is used. The soft-magnetic particles consist of soft SQ carbonyl iron powder (CIP) (BASF, Germany). The hard-magnetic particles consist of NdFeB powder (MQP-S-11-9-grade powder, Neo Materials Technology Inc., Greenwood Village, Colorado, United States). The magnetic particles occupy a total volume ratio of 30% in every sample. This allows to compare the extreme cases of pure sMRE and hMRE, as well as any other intermediate case of hybrid MRE. Such a choice is also motivated on the modelling framework where all energetic potentials are defined per unit volume. Note that matrix and particles are perfectly attached, thus no slippage occurs between them. The volumetric mixing ratio between both types of particles (soft-to-hard particles ratio) is modified considering five different cases: 1:0 (only soft), 2:1, 1:1 (equal content of soft and hard), 1:2 and 0:1 (only hard). To initiate the crosslinking, the two elastomeric phases are mixed at the ratio 1:1. Supplementary Fig. 1 shows the steps followed to manufacture the samples. Note that the initial blend is pre-heated to prevent the sedimentation of the NdFeB powder. A final step allows for the pre-magnetisation of the specimens.

Experimental procedure for shear deformation tests

A TA HR-20 rheometer with Magneto-Rheology Accessory from Waters TA Q600 (TA instrument, New Castle, DE, USA) allows axial and shear mechanical loading, axial magnetic fields and testing temperature, all controlled within a close-loop system. For the experimental analysis in 2.1, different hybrid MREs were tested under shear loading and with external magnetic actuation. The experiments considered two main mechanical loading conditions: (i) constant oscillatory shear, and (ii) frequency sweep shear. More importantly, the experiments for each mixing ratio condition were conducted on two types of samples: (1) virgin samples, i.e., specimens that have not been exposed to any external magnetic field; and (2) pre-magnetised samples, i.e., specimens exposed to an axial magnetic field of 1 T. It must be noted that such a pre-magnetising field is not enough to reach the saturation magnetisation of the hard-magnetic particles, but it is sufficient to induce some residual magnetisations. This was done on purpose as the elastomeric matrix is extremely soft and higher magnetic fields would compromise the original shape of the samples due to strong residual stresses. During the tests, axial magnetic fields of $\{0, 200, 500, 1000\}$ mT were applied on both virgin and pre-magnetised samples to evaluate their effect on the macroscopic responses. Rotational oscillations were performed at $2\,\mathrm{rad\,s^{-1}}$ with a maximum angular amplitude of 0.05 rad.

Experimental procedure for mechanically confined tests

A TA HR-20 rheometer with Magneto-Rheology Accessory from Waters TA Q600 (TA instrument, New Castle, DE, USA) provides mechanically confined studies. To this end, the MRE samples were axially confined between the lower and upper plates. Then, an axial magnetic field was applied. It was controlled with a close-loop system to ensure homogeneous fields during the test. This actuation leads to particle interactions within the sample that produces a macroscopic confined expansion. The upper plate of the rheometer, equipped with a load cell, registers the evolution of the force exerted from the MRE. Moreover, the quasi-incompressible nature of the composite limits material deformations in the transverse directions. This relates the force measured directly to the magnetic stress contribution.

The tests were first conducted on virgin samples applying magnetic ramps of $20\,\mathrm{mT\,s^{-1}}$ until reaching 1000 mT, then keeping the field constant for 75 s. Afterwards, the field was turned off for 75 s. The results are collected in Fig. 2a and b.1 for sMREs and hMREs, respectively; and in Fig. 2c1,d1,e1 for the different hybrid MREs tested. The same tests were performed on pre-magnetised samples until reaching 500 mT and under two different actuation modes: (i) direct actuation, i.e., applying the magnetic field in the same direction as the pre-magnetisation; and (ii) reverse actuation, i.e., applying the magnetic field in the opposite direction to the pre-magnetisation

Constitutive and computational framework for the microstructural model

The primary fields to be solved are the displacement field vector $\mathbf{u}$, a magnetic scalar potential ϕ and a Lagrange multiplier p related to the incompressibility condition. From the former fields, the deformation gradient and the magnetic field in the reference configuration can be computed as

$$\begin{aligned} \mathbf{F} &= \nabla_0 \mathbf{u} + \mathbf{I} \\ \mathbb{H} &= -\nabla_0 \phi = \mathbb{H}_e + \mathbb{H}_r \end{aligned} \tag{1}$$

where ∇_0 is the gradient operator with respect to the reference configuration and $\mathbf{I}$ is the second-order identity tensor. The incompressibility condition $J = 1$ is imposed by p, with $J = \det \mathbf{F}$. Note that the magnetic field is decomposed into an elastic component $\mathbb{H}_e$, and a remanent component $\mathbb{H}_r$ to account for the residual magnetisation in the hard-magnetic particles.

The field equation for the mechanical displacement field is given by the divergence of the Piola stress tensor $\mathbf{P}$ as

$$\nabla_0 \cdot \mathbf{P} = \mathbf{0}, \tag{2}$$

whereas for the magnetic problem, the Maxwell equations for the magnetostatic case are

$$\nabla_0 \times \mathbb{H} = \mathbf{0}, \quad \nabla_0 \cdot \mathbb{B} = 0, \tag{3}$$

with $\mathbb{B}$ the magnetic flux density vector in the reference configuration. The magnetic variables can be related to the magnetisation vector $\mathbb{M}$ by the constitutive relation

$$\mathbb{B} = J\mu_0 \mathbf{C}^{-1}[\mathbb{H} + \mathbb{M}], \tag{4}$$

where $\mathbf{C} = \mathbf{F}^{\mathrm{T}} \cdot \mathbf{F}$. We make use of a single total energy density function Ψ to describe the magneto-mechanical constitutive behaviour of both the

matrix and magnetic fillers at the microstructural level. The energy function is based on three contributions, i.e., mechanical, Maxwell and magnetisation energies, according to

$$\Psi(\mathbf{F},\mathbb{H}) = \Psi_{\text{mech}}(\mathbf{F}) + \Psi_{\text{maxw}}(\mathbf{F},\mathbb{H}) + \Psi_{\text{mag}}(\mathbf{F},\mathbb{H}). \tag{5}$$

The elastic energetic contribution is defined by a Neo-Hookean formulation as

$$\Psi_{\text{mech}}(\mathbf{F}) = \frac{G}{2}[I_1 - 3], \tag{6}$$

with $I_1 = \text{tr}(\mathbf{F}\cdot\mathbf{F}^{\text{T}})$ and G the shear modulus of the considered phase. The Maxwell energy describes the background magnetic energy due to the non-zero magnetic permeability of vacuum and reads as

$$\Psi_{\text{maxw}}(\mathbf{F},\mathbb{H}) = -\frac{\mu_0}{2} I_5^{\text{e}}, \tag{7}$$

with $I_5^{\text{e}} = \mathbf{F}^{-\text{T}}\cdot\mathbb{H}\cdot\mathbf{F}^{-\text{T}}\cdot\mathbb{H}$. Moreover, the contribution of the magnetisable media is additively decomposed into an energetic term $\Psi_{\text{mag,e}}$ and a remanent contribution $\Psi_{\text{mag,r}}$ as

$$\begin{aligned}\Psi_{\text{mag}}(\mathbf{F},\mathbb{H}) &= \Psi_{\text{mag,e}} + \Psi_{\text{mag,r}} \\ &= -\mu_0\left[\frac{m_{\text{s}}^2}{\chi_{\text{e}}}\log\left(\cosh\left(\frac{\chi_{\text{e}}}{m_{\text{s}}}\sqrt{I_5^{\text{e}}}\right)\right)\right] \\ &\quad + \mu_0[1+\chi_{\text{e}}]I_5^{\text{er}} + \tfrac{\mu_0}{2\chi_{\text{r}}} I_5^{\text{r}},\end{aligned} \tag{8}$$

where χ_{e} and χ_{r} are the energetic and remanent magnetic susceptibilities, respectively, and m_{s} is the magnetic saturation of the magnetisation curve of the corresponding phase. $I_5^{\text{er}} = \mathbb{H}\cdot\mathbf{C}^{-1/2}\cdot\mathbb{H}_{\text{r}}$ is the magnetic invariant presented in ref. [51], whereas $I_5^{\text{r}} = \mathbb{H}_{\text{r}}\cdot\mathbb{H}_{\text{r}}$ considers solely the remanent field. In this work, we assumed the remanent magnetic field as a constant, i.e., there is no magnetic dissipation. Therefore, the last term of the energy density can be omitted.The mechanical and magnetic constitutive equations that describe the behaviour of the microstructural phases can be directly derived from the total energy potential as

$$\begin{aligned}\mathbf{P}(\mathbf{F},\mathbb{H}) &= \tfrac{\partial\Psi}{\partial\mathbf{F}} - p\mathbf{F}^{-\text{T}}, \\ \mathbb{B}(\mathbf{F},\mathbb{H}) &= -\tfrac{\partial\Psi}{\partial\mathbb{H}}.\end{aligned} \tag{9}$$

The complete computational framework was implemented in the open source FE software FEniCS to solve the non-linear magneto-mechanical problem by an implicit monolithic integration algorithm and the FEniCS standard UFL solver with independent tolerance criteria for each contribution to the residual. The remanent magnetisation of hard magnetic particles and the macroscopic magnetic induction are applied consecutively and incrementally with the appropriate steps. Then, we created a set of representative volume elements (RVEs) matching the particles mixing ratios from the MREs in the experimental section. These consist of multi-domain RVEs that explicitly account for the carrier matrix (continuous phase) and both soft- and hard-magnetic particles (dispersed phase). Every RVE was designed to have a total amount of magnetic particles of 30 vol.%. Meshes with tetrahedral elements were defined to discretize the multiphase domain. The number of elements is comprised between 72985 and 137768, depending on the mixing ratio and other random factors. Moreover, Lagrange elements are chosen for a quadratic interpolation of the displacement and magnetic potential fields, and discontinuous Lagrange for the Lagrange multiplier for the incompressibility constraint. To simulate the isotropic distribution of the particles, we used a Monte Carlo algorithm that randomly distributes the magnetic particles within the RVE. Note that we reproduced the difference in size between soft- and hard-magnetic fillers (Fig. 3. left).

Numerical details for the cantilever beam model

Meshes with triangular elements discretise the domains of the numerical model. Depending on the case, i.e., sMRE, hybrid MRE and hMRE, the meshes for the bimorph actuator have 87374, 94519 and 76234 elements, respectively. The constitutive model of the beam layers relies on the microstructural description of the phases, i.e., matrix and particles, as incompressible media according to the description in the previous sections. The air, however, is modelled as a compressible material with a negligible stiffness with dimensions of 170×161 mm, more than ten times larger than the beam with dimensions of 10×1 mm. In addition, and according to the work by Rambausek et al.[53], a weight function for the air domain helps minimise the perturbations in the solution (see Supplementary Methods 5 for further detail). The NonlinearVariationalProblem library in FEniCS is used to numerically solve the model.

DATA AVAILABILITY

The data generated during the current study are available from the corresponding author upon reasonable request.

CODE AVAILABILITY

The code generated during the current study is available from the corresponding author upon reasonable request.

Received: 22 March 2022; Accepted: 5 July 2022;
Published online: 28 July 2022

REFERENCES

1. Moreno-Mateos, M. A. et al. Magneto-mechanical system to reproduce and quantify complex strain patterns in biological materials. *Appl. Mater. Today* **27**, 101437 (2022).
2. Son, D., Ugurlu, M. C. & Sitti, M. Permanent magnet array-driven navigation of wireless millirobots inside soft tissues. *Sci. Adv.* **7**, eabi8932 (2021).
3. Kim, Y., Parada, G. A., Liu, S. & Zhao, X. Ferromagnetic soft continuum robots. *Sci. Robotics* **4** (2019).
4. Koivikko, A., Drotlef, D.-M., Sitti, M. & Sariola, V. Magnetically switchable soft suction grippers. *Extrem. Mech. Lett.* **44**, 101263 (2021).
5. Ren, Z., Hu, W., Dong, X. & Sitti, M. Multi-functional soft-bodied jellyfish-like swimming. *Nat. Commun.* **10**, 2703 (2019).
6. Corbin, E. A. et al. Tunable and reversible substrate stiffness reveals a dynamic mechanosensitivity of cardiomyocytes. *ACS Appl. Mater. Interfaces* **11**, 20603–20614 (2019).
7. Hogan, K. J. & Mikos, A. G. Biodegradable thermoresponsive polymers: Applications in drug delivery and tissue engineering. *Polymer* **211**, 123063 (2020).
8. Uslu, F. E. et al. Engineered extracellular matrices with integrated wireless microactuators to study mechanobiology. *Adv. Mater.* **33**, 2102641 (2021).
9. Yarali, E. et al. Magneto-/electro-responsive polymers toward manufacturing, characterization, and biomedical/soft robotic applications. *Appl. Mater. Today* **26**, 101306 (2022).
10. Li, H. et al. Vibration and damping study of multifunctional grille composite sandwich plates with an imas design approach. *Compos. Part B: Eng.* **223**, 109078 (2021).
11. Bastola, A. K. & Li, L. A new type of vibration isolator based on magnetorheological elastomer. *Mater. Des.* **157**, 431–436 (2018).
12. Khayam, S. U., Usman, M., Umer, M. A. & Rafique, A. Development and characterization of a novel hybrid magnetorheological elastomer incorporating micro and nano size iron fillers. *Mater. Des.* **192**, 108748 (2020).
13. Alkhalaf, A., Hooshiar, A. & Dargahi, J. Composite magnetorheological elastomers for tactile displays: enhanced mr-effect through bi-layer composition. *Compos. Part B: Eng.* **190**, 107888 (2020).
14. Amiri, A. & Talebitooti, R. Vibration and stability analysis of fluid-conveying sandwich micro-pipe with magnetorheological elastomer core, considering modified couple stress theory and geometrical nonlinearity. *Eur. Phys. J.* **136**, 1109 (2021).
15. Behrooz, M. & Gordaninejad, F. Three-dimensional study of a one-way, flexible magnetorheological elastomer-based micro fluid transport system. *Smart Mater. Struct.* **25**, 095012 (2016).
16. Danas, K., Kankanala, S. & Triantafyllidis, N. Experiments and modeling of iron-particle-filled magnetorheological elastomers. *J. Mech. Phys. Solids* **60**, 120–138 (2012).
17. Gordaninejad, F., Wang, X. & Mysore, P. Behavior of thick magnetorheological elastomers. *J. Intell. Mater. Syst. Struct.* **23**, 1033–1039 (2012).
18. Kallio, M. *The Elastic and Damping Properties of Magnetorheological Elastomers*. 3–146 (VTT Publications, 2005).
19. Schubert, G. & Harrison, P. Large-strain behaviour of magneto-rheological elastomers tested under uniaxial compression and tension, and pure shear deformations. *Polym. Test.* **42**, 122–134 (2015).
20. Schubert, G. & Harrison, P. Equi-biaxial tension tests on magneto-rheological elastomers. *Smart Mater. Struct.* **25**, 015015 (2016).
21. Burhannuddin, N. L. et al. Physicochemical characterization and rheological properties of magnetic elastomers containing different shapes of corroded carbonyl iron particles. *Sci. Rep.* **11**, 868 (2021).

22. Lucarini, S., Hossain, M. & Garcia-Gonzalez, D. Recent advances in hard-magnetic soft composites: synthesis, characterisation, computational modelling, and applications. *Composite Struct.* **279**, 114800 (2022).
23. Stepanov, G. et al. Effect of a homogeneous magnetic field on the viscoelastic behavior of magnetic elastomers. *Polymer* **48**, 488–495 (2007).
24. Moreno, M. A., Gonzalez-Rico, J., Lopez-Donaire, M. L., Arias, A. & Garcia-Gonzalez, D. New experimental insights into magneto-mechanical rate dependences of magnetorheological elastomers. *Compos. Part B: Eng.* **224**, 109148 (2021).
25. Garcia-Gonzalez, D., Moreno, M. A., Valencia, L., Arias, A. & Velasco, D. Influence of elastomeric matrix and particle volume fraction on the mechanical response of magneto-active polymers. *Compos. Part B: Eng.* **215**, 108796 (2021).
26. Bastola, A. K. & Hossain, M. A review on magneto-mechanical characterizations of magnetorheological elastomers. *Compos. Part B: Eng.* **200**, 108348 (2020).
27. Kramarenko, E. Y. et al. Magnetic and viscoelastic response of elastomers with hard magnetic filler. *Smart Mater. Struct.* **24**, 035002 (2015).
28. Stepanov, G., Chertovich, A. & Kramarenko, E. Magnetorheological and deformation properties of magnetically controlled elastomers with hard magnetic filler. *J. Magn. Magn. Mater.* **324**, 3448–3451 (2012).
29. Stepanov, G. V., Borin, D. Y., Bakhtiiarov, A. V. & Storozhenko, P. A. Hybrid magnetic elastomers prepared on the basis of a siel-grade resin and their magnetic and rheological properties. *Phys. Sci. Rev.* 20200008 (2020).
30. Antonel, P. S. et al. Magnetic and elastic properties of CoFe2O4 - polydimethylsiloxane magnetically oriented elastomer nanocomposites. *J. Appl. Phys.* **110**, 043920 (2011).
31. Koo, J.-H., Dawson, A. & Jung, H.-J. Characterization of actuation properties of magnetorheological elastomers with embedded hard magnetic particles. *J. Intell. Mater. Syst. Struct.* **23**, 1049–1054 (2012).
32. Moreno-Mateos, M. A., Lopez-Donaire, M. L., Hossain, M. & Garcia-Gonzalez, D. Effects of soft and hard magnetic particles on the mechanical performance of ultra-soft magnetorheological elastomers. *Smart Mater. Struct.* **31**, 065018 (2022).
33. Kankanala, S. & Triantafyllidis, N. On finitely strained magnetorheological elastomers. *J. Mech. Phys. Solids* **52**, 2869–2908 (2004).
34. Bustamante, R., Dorfmann, A. & Ogden, R. Universal relations in isotropic nonlinear magnetoelasticity. *Q. J. Mech. Appl. Math.* **59**, 435–450 (2006).
35. Vu, D. & Steinmann, P. Material and spatial motion problems in nonlinear electro- and magneto-elastostatics. *Math. Mech. Solids* **15**, 239–257 (2010).
36. Pao, Y.-H. Electromagnetic forces in deformable continua. *Mech. Today* **4**, 209–305 (1978).
37. Eringen, A. C. & Maugin, G. A. Electrodynamics of Continua I. *Springer New York*, XVII–436 (1990).
38. Maugin, G. Continuum Mechanics of Electromagnetic Solids. *Elsevier* **33**, 1–598 (1988).
39. Brigadnov, I. & Dorfmann, A. Mathematical modeling of magneto-sensitive elastomers. *Int. J. Solids Struct.* **40**, 4659–4674 (2003).
40. Bustamante, R. Transversely isotropic nonlinear magneto-active elastomers. *Acta Mechanica* **210**, 183–214 (2010).
41. Bustamante, R., Dorfmann, A. & Ogden, R. On variational formulations in nonlinear magnetoelastostatics. *Math. Mech. Solids* **13**, 725–745 (2008).
42. Shariff, M., Hossain, M., Bustamante, R. & Merodio, J. Modelling the residually stressed magneto-electrically coupled soft elastic materials. *Int. J. Non-Linear Mech.* **137**, 103802 (2021).
43. Dorfmann, A. & Ogden, R. Nonlinear magnetoelastic deformations of elastomers. *Acta Mechanica* **167**, 13–28 (2004).
44. Haldar, K., Kiefer, B. & Menzel, A. Finite element simulation of rate-dependent magneto-active polymer response. *Smart Mater. Struct.* **25**, 104003 (2016).
45. Haldar, K. Constitutive modeling of magneto-viscoelastic polymers, demagnetization correction, and field-induced poynting effect. *Int. J. Eng. Sci.* **165**, 103488 (2021).
46. Saxena, P., Hossain, M. & Steinmann, P. A theory of finite deformation magneto-viscoelasticity. *Int. J. Solids Struct.* **50**, 3886–3897 (2013).
47. Saxena, P., Hossain, M. & Steinmann, P. Nonlinear magneto-viscoelasticity of transversally isotropic magneto-active polymers. *Proc. Mathematical, Physical, and Engineering Sciences* (The Royal Society, 2014).
48. Ethiraj, G. & Miehe, C. Multiplicative magneto-elasticity of magnetosensitive polymers incorporating micromechanically-based network kernels. *Int. J. Eng. Sci.* **102**, 93–119 (2016).
49. Garcia-Gonzalez, D. & Hossain, M. Microstructural modelling of hard-magnetic soft materials: dipole-dipole interactions versus zeeman effect. *Extrem. Mech. Lett.* **48**, 101382 (2021).
50. Liu, Y., Chen, S., Tan, X. & Cao, C. A finite element framework for magneto-actuated large deformation and instability of slender magneto-active elastomers. *Int. J. Appl. Mech.* **12**, 2050013 (2020).
51. Mukherjee, D., Rambausek, M. & Danas, K. An explicit dissipative model for isotropic hard magnetorheological elastomers. *J. Mech. Phys. Solids* **151**, 104361 (2021).
52. Mukherjee, D. & Danas, K. A unified dual modeling framework for soft and hard magnetorheological elastomers. *Int. J. Solids Struct.*111513 (2022).
53. Rambausek, M., Mukherjee, D. & Danas, K. A computational framework for magnetically hard and soft viscoelastic magnetorheological elastomers. *Computer Methods Appl. Mech. Eng.* **391**, 114500 (2022).
54. Javili, A., Chatzigeorgiou, G. & Steinmann, P. Computational homogenization in magneto-mechanics. *Int. J. Solids Struct.* **50**, 4197–4216 (2013).
55. Kalina, K. A., Metsch, P. & Kästner, M. Microscale modeling and simulation of magnetorheological elastomers at finite strains: a study on the influence of mechanical preloads. *Int. J. Solids Struct.* **102-103**, 286–296 (2016).
56. Kalina, K. A., Metsch, P., Brummund, J. & Kästner, M. A macroscopic model for magnetorheological elastomers based on microscopic simulations. *Int. J. Solids Struct.* **193-194**, 200–212 (2020).
57. Keip, M.-A. & Rambausek, M. A multiscale approach to the computational characterization of magnetorheological elastomers. *Int. J. Numer. Methods Eng.* **107**, 338–360 (2016).
58. Keip, M.-A. & Sridhar, A. A variationally consistent phase-field approach for micromagnetic domain evolution at finite deformations. *J. Mech. Phys. Solids* **125**, 805–824 (2019).
59. Lefévre, V., Danas, K. & Lopez-Pamies, O. Two families of explicit models constructed from a homogenization solution for the magnetoelastic response of mres containing iron and ferrofluid particles. *Int. J. Non-Linear Mech.* **119**, 103362 (2020).
60. Leonard, M., Wang, N., Lopez-Pamies, O. & Nakamura, T. The nonlinear elastic response of filled elastomers: experiments vs. theory for the basic case of particulate fillers of micrometer size. *J. Mech. Phys. Solids* **135**, 103781 (2020).
61. Metsch, P. et al. Magneto-mechanical coupling in magneto-active elastomers. *Materials* **14**, 434 (2021).
62. Miehe, C., Vallicotti, D. & Teichtmeister, S. Homogenization and multiscale stability analysis in finite magneto-electro-elasticity. application to soft matter ee, me and mee composites. *Computer Methods Appl. Mech. Eng.* **300**, 294–346 (2016).
63. Mukherjee, D., Bodelot, L. & Danas, K. Microstructurally-guided explicit continuum models for isotropic magnetorheological elastomers with iron particles. *Int. J. Non-Linear Mech.* **120**, 103380 (2020).
64. Castañeda, P. P. & Galipeau, E. Homogenization-based constitutive models for magnetorheological elastomers at finite strain. *J. Mech. Phys. Solids* **59**, 194–215 (2011).
65. Linke, J. M., Borin, D. Y. & Odenbach, S. First-order reversal curve analysis of magnetoactive elastomers. *RSC Adv.* **6**, 100407–100416 (2016).
66. Vaganov, M., Borin, D., Odenbach, S. & Raikher, Y. Effect of local elasticity of the matrix on magnetization loops of hybrid magnetic elastomers. *J. Magn. Magn. Mater.* **459**, 92–97 (2018).
67. Becker, T., Zimmermann, K., Borin, D., Stepanov, G. & Storozhenko, P. Dynamic response of a sensor element made of magnetic hybrid elastomer with controllable properties. *J. Magn. Magn. Mater.* **449**, 77–82 (2018).
68. Borin, D., Stepanov, G. & Dohmen, E. Hybrid magnetoactive elastomer with a soft matrix and mixed powder. *Arch. Appl. Mech.* **89**, 105–117 (2019).
69. Borin, D., Odenbach, S. & Stepanov, G. Stress induced by the striction of hybrid magnetoactive elastic composites. *J. Magn. Magn. Mater.* **470**, 85–88 (2019).
70. Sanchez, P. A., Stolbov, O. V., Kantorovich, S. S. & Raikher, Y. L. Modeling the magnetostriction effect in elastomers with magnetically soft and hard particles. *Soft Matter* **15**, 7145–7158 (2019).
71. Becker, T. I., Stolbov, O. V., Borin, D. Y., Zimmermann, K. & Raikher, Y. L. Basic magnetic properties of magnetoactive elastomers of mixed content. *Smart Mater. Struct.* **29**, 075034 (2020).
72. Bastola, A. K. & Hossain, M. The shape - morphing performance of magnetoactive soft materials. *Mater. Des.* **211**, 110172 (2021).
73. Bayaniahangar, R., Ahangar, S. B., Zhang, Z., Lee, B. P. & Pearce, J. M. 3-d printed soft magnetic helical coil actuators of iron oxide embedded polydimethylsiloxane. *Sens. Actuators B: Chem.* **326**, 128781 (2021).
74. Ceylan, H. et al. 3d-printed biodegradable microswimmer for theranostic cargo delivery and release. *ACS Nano* **13**, 3353–3362 (2019).
75. Huang, H.-W., Sakar, M. S., Petruska, A. J., Pané, S. & Nelson, B. J. Soft micromachines with programmable motility and morphology. *Nat. Commun.* **7**, 12263 (2016).
76. Schmidt, J., Marques, M. R. G., Botti, S. & Marques, M. A. L. Recent advances and applications of machine learning in solid-state materials science. *npj Computational Mater.* **5**, 83 (2019).
77. Kumar, S., Tan, S., Zheng, L. & Kochmann, D. M. Inverse-designed spinodoid metamaterials. *npj Computational Mater.* **6**, 73 (2020).
78. Liang, Q. et al. Benchmarking the performance of bayesian optimization across multiple experimental materials science domains. *npj Computational Mater.* **7**, 188 (2021).

ACKNOWLEDGEMENTS

The authors acknowledge support from the European Research Council (ERC) under the European Union's Horizon 2020 research and innovation programme (grant agreement No. 947723, project: 4D-BIOMAP). M.H. and D.G.G. acknowledge support from MCIN/AEI/10.13039/501100011033 under Grant number PID2020-117894GA-I00. M.A.M.M. acknowledges support from the Ministerio de Ciencia, Innovacion y Universidades, Spain (FPU19/03874). D.G.G. acknowledges support from the Talent Attraction grant (CM 2018- 2018-T2/IND-9992) from the Comunidad de Madrid. M.H. acknowledges the funding through an EPSRC Impact Acceleration Award (EP/R511614/1).

AUTHOR CONTRIBUTIONS

All authors conceived the research. M.A.M.M. performed the experiments. M.A.M.M. and D.G.G. implemented the computational model and wrote the original manuscript. All authors conducted the formal analysis, discussion and revised the paper.

COMPETING INTERESTS

The authors declare no competing interests.

ADDITIONAL INFORMATION

Supplementary information The online version contains supplementary material available at https://doi.org/10.1038/s41524-022-00844-1.

Correspondence and requests for materials should be addressed to Miguel Angel Moreno-Mateos or Daniel Garcia-Gonzalez.